

Article

UIO-66/Ag/TiO₂ Nanocomposites as Highly Active SERS Substrates for Quantitative Detection of Hexavalent Chromium

Zixiang Ben, Guangran Ma and Fugang Xu *

College of Chemistry and Chemical Engineering, Jiangxi Normal University, Nanchang 330022, China

* Correspondence: fgxu@jxnu.edu.cn

Abstract: Sensitive determination of Cr(VI) is of great importance as this is one of the most toxic heavy metal ions in the environment. In this work, a metal–organic framework (MOF) material, UIO-66 (University of Oslo, UIO), was introduced for the first time to develop a composite substrate, UIO-66/Ag/TiO₂, for the sensitive SERS detection of Cr(VI) in water. The composition, morphology, crystal structure and optical property of the UIO-66/Ag/TiO₂ were characterized by SEM, XRD, EDX, UV-Vis and Raman spectroscopy. The control experiment revealed the introduction of UIO-66 and TiO₂ can improve the adsorption to Cr ions and thus greatly enhance the SERS signal of Cr(VI) on this composite substrate. The SERS signal can also be tuned by changing the dosage of TiO₂. Under optimized conditions, UIO-66/Ag/TiO₂ was used to detect Cr(VI) in water with different concentrations, which showed high sensitivity and good stability. The SERS signals showed a linear increase as the concentration of Cr(VI) increases from 5×10^{-9} M to 5×10^{-6} M. The detection limit was 5 nM, which was lower than the safe drinking water standard of the US Environmental Protection Agency (1 μ M). Detection of Cr(VI) in the range of 1×10^{-7} M to 5×10^{-6} M in real lake water was also achieved. These results demonstrate the great potential of UIO-66/Ag/TiO₂ composites as SERS substrates for the trace determination of Cr(VI) in the environmental field.

Keywords: surface enhanced Raman scattering; metal–organic framework; composite material; enhancement substrate; Cr(VI); environment analysis; chemical sensor

**Citation:** Ben, Z.; Ma, G.; Xu, F.UIO-66/Ag/TiO₂ Nanocomposites as Highly Active SERS Substrates for Quantitative Detection of Hexavalent Chromium. *Chemosensors* **2023**, *11*, 315. <https://doi.org/10.3390/chemosensors11060315>

Academic Editor: Barbara Palys

Received: 13 April 2023

Revised: 15 May 2023

Accepted: 22 May 2023

Published: 24 May 2023



Copyright: © 2023 by the authors. Licensee MDPI, Basel, Switzerland. This article is an open access article distributed under the terms and conditions of the Creative Commons Attribution (CC BY) license (<https://creativecommons.org/licenses/by/4.0/>).

1. Introduction

Over the past few decades, hexavalent chromium Cr(VI) has been widely used in industries such as electroplating [1], pigment [2], printing [3], tanning [4], wood preservation [5] and steel production [6], resulting in its growth in the environment at an alarming level. According to a previous report [7], heavy metal ions are highly toxic environmental pollutants, among which Cr(VI) has been reported as a carcinogen and is one of the relatively common heavy metal ions in the environment. Due to its solubility in water and high oxidation potential, after Cr(VI) enters the body, Cr(VI) can penetrate biofilms and cause a variety of chronic and acute diseases ranging from dermatitis and edema to lung and kidney cancer [8]. As a result, the World Health Organization (WHO) has set the maximum limit for Cr(VI) contamination in groundwater at 0.17 μ M, and the Environmental Protection Agency (EPA) has set the standard for total chromium at 1 μ M [9] to promote the public health benefits of chromium in drinking water.

Detection of Cr can be achieved by traditional methods such as inductively coupled plasma mass spectrometry (ICP-MS) and atomic absorption spectrometry (AAS) [10–15]. These methods require large experiments, complex operations and time-consuming measurements, although they display high sensitivity and accuracy. Therefore, there is still an urgent need to develop an efficient and rapid method for detecting Cr(VI) in water.

Surface-enhanced Raman scattering (SERS) technology has the advantages of high sensitivity, fast detection speed, non-destructive detection and no sample pretreatment [16], and it is often used to identify harmful substances including organic dyes, pesticides and

heavy metal ions [17–19]. SERS detection of Cr can be divided into the indirect approach and the direct approach [20–24]. For the indirect approach, the SERS signal of report molecules instead of the signal from Cr(VI) is recorded. As the reporter's signal intensity is changed in the presence of Cr(VI), indirect detection of Cr(VI) is achieved [20,21]. The indirect approach often displays high sensitivity, but the ingenious design of the report molecule and surface modifier makes the preparation of the SERS probe complex. For direct detection, the SERS signal of Cr(VI) from symmetric and asymmetric stretching vibrations of the Cr-O bond was recorded for detection of Cr(VI). Compared to the indirect approach, direct detection is simple as no report molecule is needed. In addition, direct detection may be more accurate due to the fingerprint characteristics of SERS spectra from Cr(VI) itself. However, the sensitivity of this approach is poor on bare noble metal SERS substrates due to the poor affinity of Cr(VI) to noble metal surfaces. Fortunately, by rational combination with other functional materials, high adsorption to heavy metal and thus good sensing sensitivity can also be achieved. For example, Wang's research group prepared a $\text{Fe}_3\text{O}_4@m\text{-ZrO}_2@\text{Ag}$ nanostructure [22]. Porous ZrO_2 was not only conducive to the load of AgNPs, but also conducive to the adsorption of Cr(VI) due to the abundant hydroxyl groups on its surface, thus improving the SERS detection ability for Cr(VI). Wang et al. proposed a rapid quantitative Cr(VI) method based on $\text{Mg}(\text{NO}_3)_2$ -induced polymerization of AgNPs [23], whose SERS signal was attributed to the Cr-O bond. Therefore, the SERS technique integrated with new functional materials, especially those with high affinity or adsorption to Cr(VI), is a promising way for sensitive detection of Cr(VI) in the environment.

Recently, metal-organic frameworks (MOFs) and metal oxides have shown great promise for the adsorption or sensing of Cr(VI) and other pollutants [24,25]. The large surface area, adjustable pore size and attractive chemical diversity of MOFs endow them with high affinity and adsorption to Cr(VI). For example, a Fe^{2+} -involved MOF+ technique was developed for Cr removal, showing an extraordinary adsorption capacity of 796 Cr mg/g [26]. A Zr^{4+} -MOF was synthesized for Cr removal and luminescence sensing. The porous structure and Zr-bonded hydroxides in the framework endow it with a high capture ability for Cr(VI) (149 mg/g) [27]. Interestingly, such high adsorption of MOFs to Cr(VI) has not been used for SERS detection of Cr(VI). Besides MOFs, metal oxides such as TiO_2 and ZrO_2 also show a high affinity to Cr(VI). The strong coordinating interaction between ZrO_2 and CrO_4^{2-} or $\text{Cr}_2\text{O}_7^{2-}$ has been used to improve the SERS signal of Cr(VI) on ZrO_2 -based composite substrates [9,22]. An indirect approach for SERS detection of Cr(VI) was developed [28], where the interaction between Cr(VI) and Ti(IV) atoms with unfilled valence orbitals at the TiO_2 surface endows the method a good selectivity. TiO_2 combined with Au was also used to improve the SERS signal of Cr(VI) [29]. The hydroxyl group on the TiO_2 is believed to play a major role in enhancing affinity to Cr(VI). Based on these reports, it is expected that a rational combination of a traditional Au- or Ag-based SERS substrate with an MOF and metal oxide may greatly improve the SERS sensing performance, which is seldom reported.

In this study, we developed a new MOF-based SERS substrate composed of UIO-66/Ag/TiO_2 , which was the first time that MOF material was applied to the SERS detection of Cr(VI). UIO-66, with a large surface area and high adsorption to Cr(VI), was used as support. AgNPs with high electromagnetic enhancement ability for SERS signaling were loaded onto UIO-66 to form UIO-66/Ag. Finally, TiO_2 colloids were assembled onto UIO-66/Ag to form UIO-66/Ag/ TiO_2 . Due to the synergy of these components, the composite substrate UIO-66/Ag/ TiO_2 shows significant adsorption to Cr(VI), and consequently, highly sensitive SERS detection of Cr(VI) was achieved. Such a composite substrate was successfully used for quantitative and trace detection of Cr(VI) in aqueous solutions and actual samples, which shows great promise for environment analysis.

2. Materials and Methods

2.1. Chemicals and Materials

Zirconium chloride ($ZrCl_4$, AR), 1,4-dicarboxybenzene (BDC, AR), polyvinylpyrrolidone (PVP K30), silver nitrate ($AgNO_3$, AR), sodium chloride (NaCl, AR), sodium nitrate ($NaNO_3$, AR), sodium carbonate (Na_2CO_3 , AR), sodium sulfate anhydrous (Na_2SO_4 , AR), potassium dichromate ($K_2Cr_2O_7$, AR), N, N-dimethylformamide (DMF), methanol, acetic acid and tetrabutyl titanate (TBT, 98%) were purchased from Aladdin chemical reagent company (Shanghai, China). Deionized water purified by a Millipore system was used as a solvent throughout the experiment.

2.2. Apparatus and Measurements

The material microstructure was imaged using a scanning electron microscope (SEM, S-3400, Hitachi, Tokyo, Japan); the absorption capacity of the material for Cr(VI) was assessed with an ultraviolet–visible spectrometer (UV-3900, Hitachi, Tokyo, Japan). The SERS signal was recorded with a 633 nm He-Ne laser (LABRAM-HR, Horiba, Palaiseau, France), the structure of the material was measured with an X-ray diffractometer (XRD. MINIFLEX 600, Rigaku, Akishima, Japan) and the composition of the material was characterized by X-ray photoelectron spectrometry (XPS, Escalab, Shimadzu, Kyoto, Japan).

2.3. Preparation of UIO-66/Ag

UIO-66/Ag was made according to a published report [30]. Briefly, 104.9 mg of zirconium(IV) chloride, 81.5 mg of terephthalic acid and 12 mL of acetic acid were added to 100 mL of dimethylformamide (DMF) solution. The mixed solution was transferred to an autoclave and heated in an oven at 120 °C for 24 h. The reaction product was centrifuged at $10,000 \times g$ rpm for 5 min and washed with a methanol–DMF mixture. The precipitate was then dried in a vacuum oven to obtain a white UIO-66 powder. Then, 20 mg of UIO-66 and 40 mg of silver nitrate were dispersed in 20 mL of DMF. The mixture solution was then transferred to an autoclave and reacted at 160 °C for 3 h. The cooled solution was centrifuged at $10,000 \times g$ rpm for 5 min and washed three times with methanolic DMF solution. The obtained material was then dried in an oven.

2.4. Preparation of TiO_2

First, 12.5 mL of a solution of tetrabutyl titanate (98%) was added to 4 mL of isopropanol. The mixture was shaken until a homogeneous solution appeared. Then, the mixture was added dropwise to a solution containing 150 mL of deionized water and 2 mL of HNO_3 under vigorous stirring at 70–80 °C until a clear colloid was obtained [29].

2.5. Preparation of UIO-66/Ag/ TiO_2

Twenty milligrams of UIO-66/Ag powder was ultrasonically dispersed in 5 mL of 200 mg of PVP methanol solution and stirred at room temperature for 12 h. The solution at the end of the reaction was centrifuged at $10,000 \times g$ rpm for 5 min and washed three times with methanol solution. Then the obtained material was dried in an oven. After centrifugal drying, 10 mg of sample was taken with 10 mL of TiO_2 colloid and stirred for 12 h. The final sample was obtained by centrifugal drying.

2.6. Raman Spectroscopic Analysis

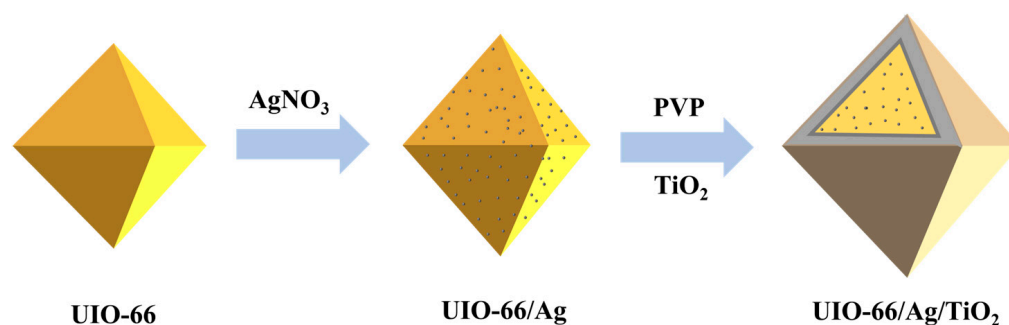
Potassium dichromate solutions were used for SERS sensitivity assessment. Potassium dichromate solutions with different concentrations from 5×10^{-6} to 5×10^{-9} M were tested. Confocal Raman spectroscopy was used for all SERS experiments. A $50 \times$ objective lens was used, and the laser excitation wavelength was 633 nm. The laser power was ~ 0.2 mW. The integration time was 10 s. First, 1 mg of UIO-66/Ag/ TiO_2 was ultrasonically dispersed in 1 mL of deionized water. Then, 200 μ L of the UIO-66/Ag/ TiO_2 suspension was added to 1 mL of different concentrations of Cr(VI) aqueous solution, and the mixed solution was shaken at room temperature for 1 h to ensure complete adsorption. Then, the

mixed solutions were centrifuged at $5000\times g$ rpm for 10 min and washed several times with ultrapure water. Finally, the precipitate was dispersed in 0.5 mL of ultrapure water for SERS analysis.

3. Results

3.1. Fabrication and Characterization of UIO-66/Ag/TiO₂ Nanocomposites

The formation of UIO-66/Ag/TiO₂ nanocomposites involved several steps. As shown in Scheme 1, UIO-66 nanoparticles (average size in the range of 1.5–2.5 μm) were synthesized by the solvothermal method, and it could be seen that the synthesized UIO-66 surface was well crystallized. Then, UIO-66/Ag composite nanoparticles were synthesized by the solvothermal method; a layer of AgNPs loaded on the surface of UIO-66 can be clearly seen in Figure 1a–c. AgNPs were prepared by reducing silver nitrate with DMF as the reducing agent to avoid damage to the UIO-66 framework. Compared with the AgNPs synthesized alone, the agglomeration of AgNPs loaded on UIO-66 was significantly reduced, which may be related to the porous structure of UIO-66 and the large specific surface area for adsorption of AgNPs. The AgNPs were embedded in the pores of UIO-66, which reduced the mobility of AgNPs and allowed the AgNPs to be uniformly dispersed on the surface of UIO-66. Finally, TiO₂ colloids were self-assembled onto UIO-66/Ag to form the final product UIO-66/Ag/TiO₂. As can be seen in Figure 1d, the presence of both Ti and Ag elements shows the successful synthesis of UIO-66/Ag/TiO₂. Moreover, a large amount of Ag elements can be seen according to the elemental content in Figure 1d, which proves that a large amount of AgNPs are loaded on the MOF surface to form a stable and uniform hot spot.



Scheme 1. Schematic illustration of the fabrication process of UIO-66/Ag/TiO₂.

In Figure 2, the characteristic XRD peaks of UIO-66 (black line) are located at 7.3° and 8.4° ; these peaks are consistent with those reported in the literature [31]. For UIO-66/Ag, new peaks at 38.20° , 44.40° , 64.60° and 77.40° attributed to the (111), (200), (220) and (311) crystal silver planes appear [30]. In addition, all diffraction peaks are very sharp, which indicates that the UIO-66/AgNPs composites have high crystallinity. For the final composite, characteristic peaks at 25.3° , 37.8° and 48° corresponding to (101), (004) and (200) crystal planes of TiO₂ can be observed [32], implying the successful formation of UIO-66/Ag/TiO₂.

Figure 3 shows the main elements of the material, namely C, O, Zr, Ag and Ti. The C1s spectrum is divided into three peaks of 284.4, 285.8 and 288.2 eV, which are attributed to C-C, C-O and C=C groups on UIO-66 [33]. The O1s spectrum is divided into two peaks of 529.6 and 531.4 eV, which are attributed to Ti-O in TiO₂ and C-O/C=O groups [34]. Zr3d was divided into two peaks of 182.1 and 184.5 eV, which were attributed to Zr3d_{5/2} and Zr3d_{3/2} of the Zr in UIO-66 [35]. Ag3d was divided into two peaks of 368.0 and 374.1 eV, with a difference of about 6 eV between the two peaks, confirming that AgNPs are present in the zero valence state and further confirming the loading of AgNPs on UIO-66 [36]. Ti2p was divided into two peaks: Ti2p_{3/2} and Ti2p_{1/2} at 458.4 and 464.1 eV [37]. The successful synthesis of UIO-66/Ag/TiO₂ was confirmed by the above SEM, EDX, XRD and XPS results.

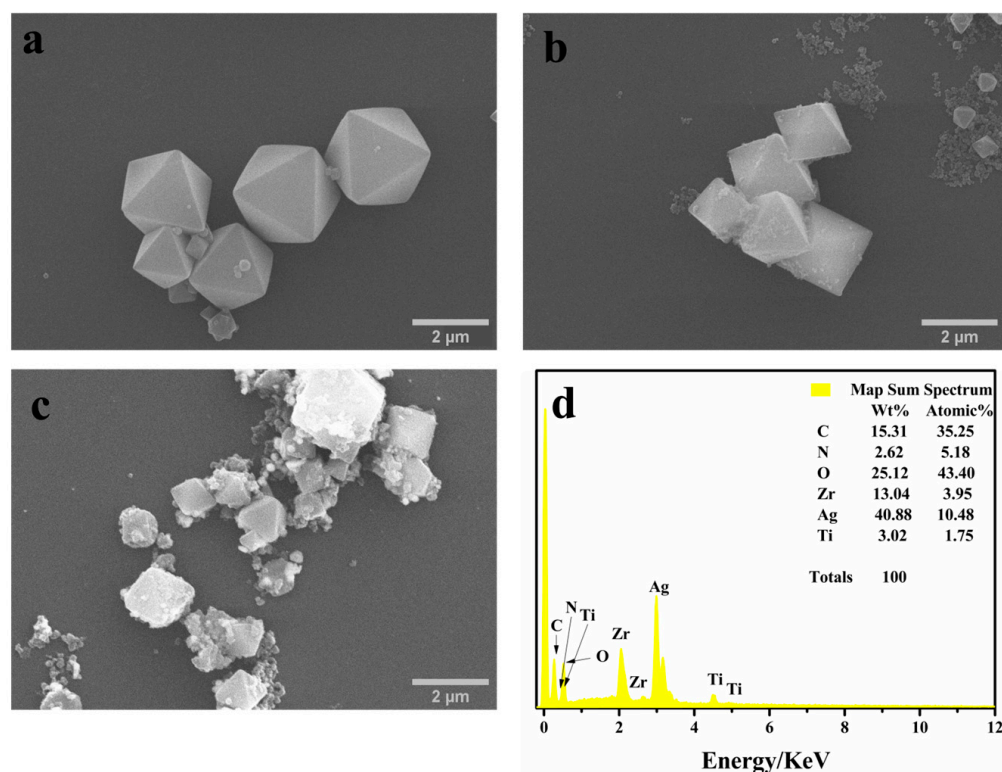


Figure 1. SEM images of (a) UIO-66, (b) UIO-66/Ag and (c) UIO-66/Ag/TiO₂; (d) EDX images of UIO-66/Ag/TiO₂.

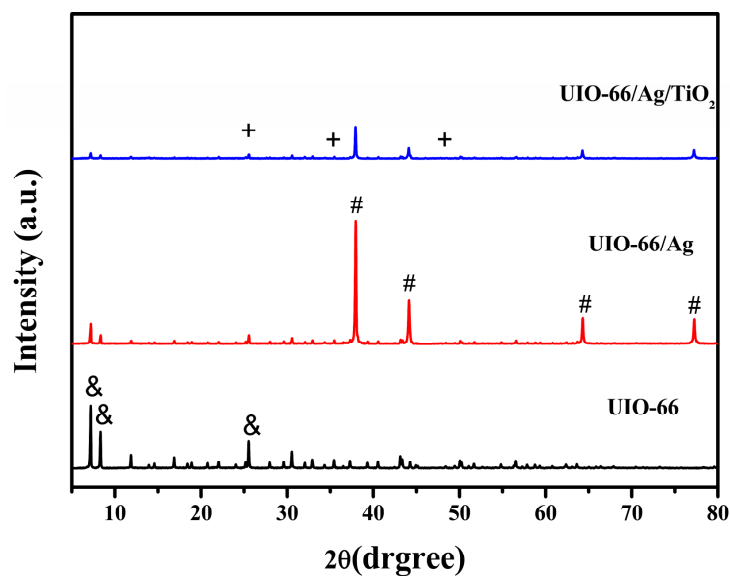


Figure 2. XRD pattern of different materials. Note that peaks marked with symbols “&”, “#” and “+” represent the peaks from UIO-66, AgNPs and TiO₂, respectively.

3.2. SERS Performance

According to the electromagnetic mechanism (EM) and chemical mechanism (CM) of SERS, a strong SERS signal will be produced when probe molecules are directly adsorbed on or very close to the surface of the enhancement substrate. So, enhancing the adsorption of the substrate to target molecules is important for a strong SERS signal. Here, an MOF and TiO₂ were both used to enhance the adsorption to Cr(VI). As Figure 4 shows, pristine potassium dichromate solution displays an absorption peak at 352 nm [38]. After incuba-

tion with UIO-66, the UV absorption peak of Cr(VI) decreases significantly (red curve), confirming that MOF materials with large specific surface area have strong adsorption capacity. The UV absorption peak of Cr(VI) further decreases slightly when UIO-66/Ag is used for incubation with the Cr(VI) solution (blue curve). This result confirms that bare noble metal only displays a low affinity to Cr(VI). The UV absorption peak of Cr(VI) further significantly decreases when UIO-66/Ag/TiO₂ is used for incubation with Cr(VI), indicating TiO₂ can obviously improve the ability of adsorption to Cr(VI). The enhanced adsorption can be ascribed to the plentiful hydroxyl groups of TiO₂ colloids, as detailed in previous reports [28,29]. The results in Figure 4 indicate bare silver nanoparticles show poor adsorption to Cr(VI), while introducing a MOF and TiO₂ can significantly improve the adsorption to Cr(VI) owing to the large specific area of the MOF and abundant hydroxyl groups of TiO₂ for Cr(VI) binding. The high adsorption observed on UIO-66/Ag/TiO₂ is beneficial for obtaining a strong SERS signal for sensitive detection of Cr(VI).

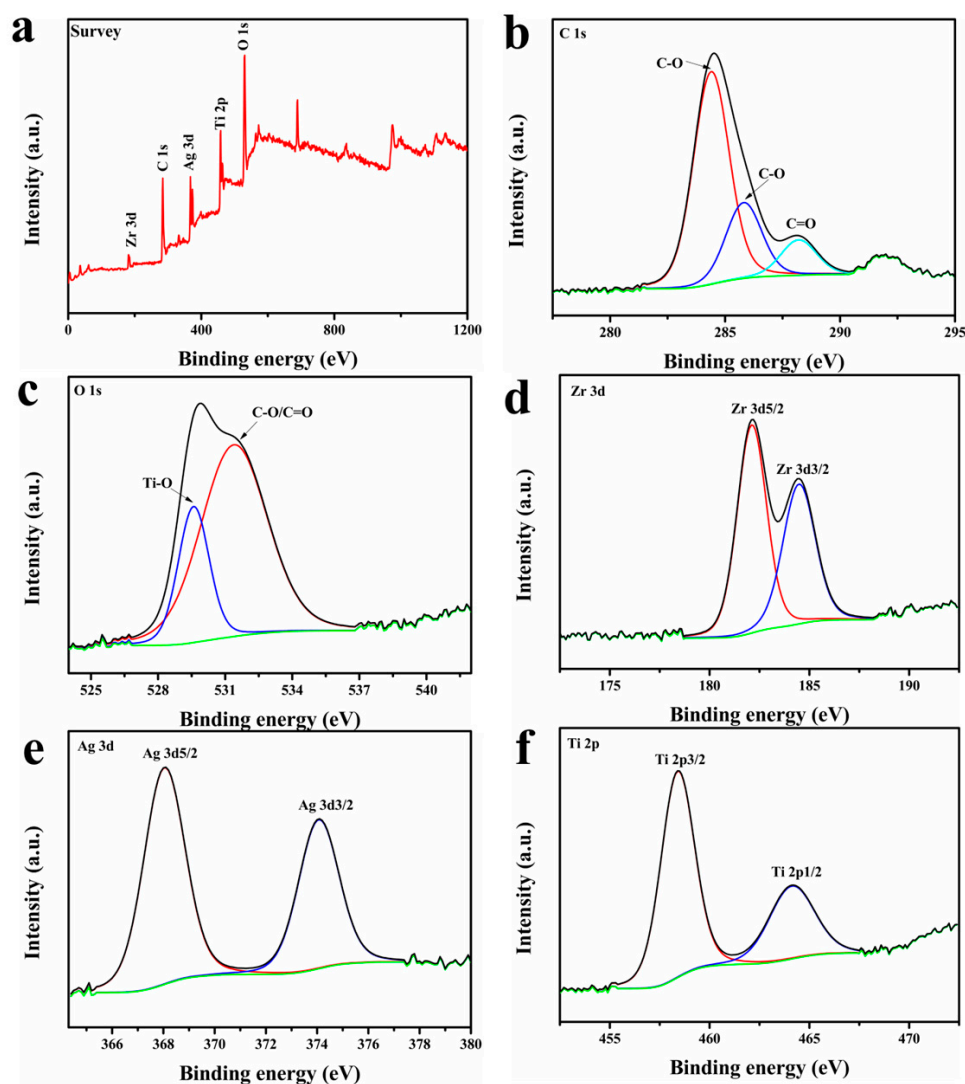


Figure 3. High-resolution XPS spectra of (a) the survey scan, (b) C 1s, (c) O 1s, (d) Zr 3d, (e) Ag 3d and (f) Ti 2p from UIO-66/Ag/TiO₂.

Here, we compare the original Raman signals of the above materials and their direct SERS response in the presence of Cr(VI). Figure 5 shows the original Raman characteristic peaks of UIO-66 (black curve), UIO-66/Ag (red curve) and UIO-66/Ag/TiO₂ (blue curve). The peaks at 852 cm⁻¹, 1130 cm⁻¹ and 1607 cm⁻¹ are ascribed to the out-of-plane bending vibration of C-H on the aniline ring, C-C-C bending vibration and C=C stretching of the

aromatic ring from UIO-66. The Raman signal of UIO-66 was enhanced on UIO-66/Ag owing to the electromagnetic enhancement of Ag. The signal of UIO was slightly reduced on UIO-66/Ag/TiO₂. This is helpful for improving the signal-to-noise ratio, although the detailed mechanism for the reduced signal of UIO is not clear at present. In the presence of Cr(VI), the characteristic peak signal of Cr(VI) was not observed on the substrate UIO-66, indicating UIO-66 was not a SERS-active substrate. For UIO-66/Ag and UIO-66/Ag/TiO₂, the characteristic peak of Cr(VI) at 798 cm⁻¹ can be clearly observed. This peak comes from the stretching vibration of the Cr-O bond. For UIO-66/Ag substrate, a broad shoulder peak was observed at about 798 cm⁻¹ in addition to the enhanced signal from UIO-66 at 852 cm⁻¹, 1130 cm⁻¹ and 1607 cm⁻¹ [39]. The signal from UIO-66 produces a large background, which makes it difficult to distinguish the signal of Cr(VI). This may lead to a low signal-to-noise ratio and is not good for trace analysis of Cr(VI). Nevertheless, as shown in Figure 5b, it can still be seen that the SERS signal intensity of the Cr-O bond of UIO-66/Ag at a Raman shift of 798 cm⁻¹ decreases as the concentration of Cr(VI) decreases. Compared with UIO-66/Ag, the SERS signal of Cr(VI) is stronger on UIO-66/Ag/TiO₂, and the spectrum is clearer as no other peaks from materials are observed due to the coverage of TiO₂. Thus, UIO-66/Ag/TiO₂ displays a higher signal-to-noise ratio for Cr(VI) sensing. Based on the above comparison of the adsorption performance and SERS performance of UIO-66, UIO-66/Ag and UIO-66/Ag/TiO₂, it can be seen that the UIO-66/Ag/TiO₂ substrate is the best SERS substrate among them for the detection of Cr(VI). The high SERS performance of the UIO-66/Ag/TiO₂ can be ascribed to the synergy among different components. The plentiful pores of UIO bring high adsorption to Cr, while its large surface area provides more sites for anchoring highly SERS-active AgNPs. The uniform and dense AgNPs bring great SERS enhancement due to their extraordinary electromagnetic enhancement ability. Finally, the addition of TiO₂ not only improves the adsorption to Cr(VI), but also reduces the background signal, which leads to greatly enhanced performance. These results further confirm that a rational combination of Au or Ag with functional materials is beneficial for improving SERS sensing performance.

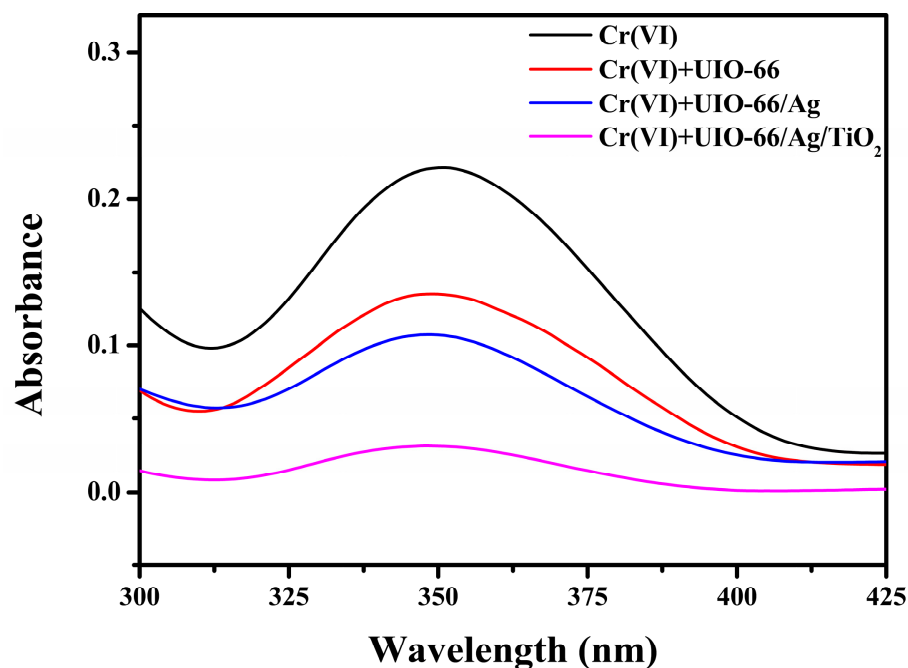


Figure 4. UV-vis spectra of Cr(VI) aqueous solution (10^{-6} M), after being incubated with UIO-66, UIO-66/Ag and UIO-66/Ag/TiO₂.

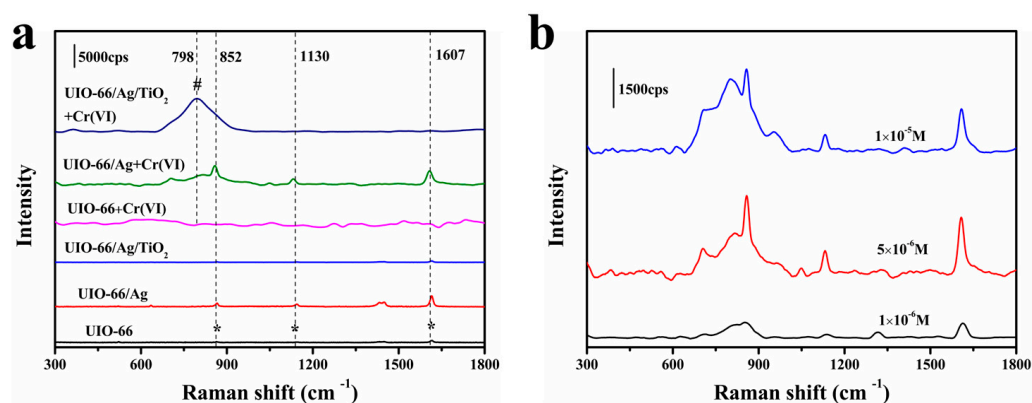


Figure 5. (a) Raman spectra of UIO-66, UIO-66/Ag and UIO-66/Ag/TiO₂ and their SERS response in presence of Cr(VI); * represents the Raman peak of UIO-66 and # represents the Raman peak of Cr(VI). (b) SERS spectra of different concentrations (1×10^{-5} – 1×10^{-6} M) of Cr(VI) on the UIO-66/Ag.

As TiO₂ is important in enhancing adsorption and improving the signal-to-noise ratio, the effect of different volumes of TiO₂ on the SERS response of UIO-66/Ag/TiO₂ was studied. Figure 6 shows that the SERS signal of Cr(VI) on UIO-66/Ag/TiO₂ increases as the TiO₂ suspension volume changes from 5 to 10 mL and then decreases when more TiO₂ is used for integration with UIO-66/Ag. So, 10 mL of TiO₂ colloids combined with UIO-66/Ag had the strongest SERS signal for Cr(VI). This is reasonable as the addition of TiO₂ may introduce two effects: enhancing adsorption to Cr(VI) and increasing the distance between AgNPs and surface-adsorbed Cr(VI). When the dosage of TiO₂ exceeded 10 mL, the TiO₂ film resulted in an increased distance of adsorbed Cr(VI) to the AgNPs, which significantly reduced the LSPR effect of AgNPs and thus reduced the SERS signal. UIO-66/Ag/TiO₂ is similar to the core–shell structure of a noble metal–MOF due to the adjustment of the thickness of the outer shell layer and thus the SERS intensity. This also proves, on the other hand, that the addition of TiO₂ can enhance the adsorption of Cr(VI), although it obscures part of the hot spot of AgNPs, which further enhances the SERS signal that should be reduced. Therefore, in the following work, 10 mL TiO₂ suspension was used as the optimized dosage to prepare the composite UIO-66/Ag/TiO₂ for SERS detection of Cr in various samples.

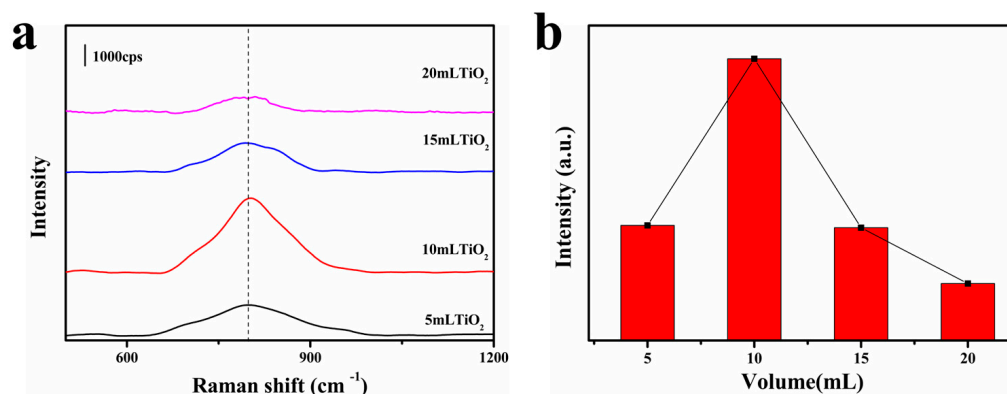


Figure 6. (a) SERS intensity of Cr(VI) aqueous solution (5×10^{-6} M) with different volumes of TiO₂ colloid. (b) SERS intensity of characteristic peaks at 798 cm⁻¹.

The optimized composite substrate UIO-66/Ag/TiO₂ was first used for the detection of Cr(VI) in a standard solution. As shown in Figure 7, a clear SERS characteristic peak of Cr(VI) was observed at 5×10^{-6} M level for UIO-66/Ag/TiO₂. The SERS intensity of this peak decreased with decreasing concentration of Cr(VI). The results showed that the characteristic peak of Cr(VI) was still identifiable at the concentration of 5×10^{-9} M,

indicating that UIO-66/Ag/TiO₂ could detect Cr(VI) sensitively. In addition, the peak intensity (*I*) showed a good linear correlation with the logarithm of the concentration (*lgC*) in the concentration range of 5×10^{-6} – 5×10^{-9} M. The regression equation was $I = 1190.8 \lg C + 10,014.2$; thus, the quantitative analysis of this complex substrate was feasible. The results further demonstrate the great potential of the substrate for the quantitative detection of Cr(VI) in real samples.

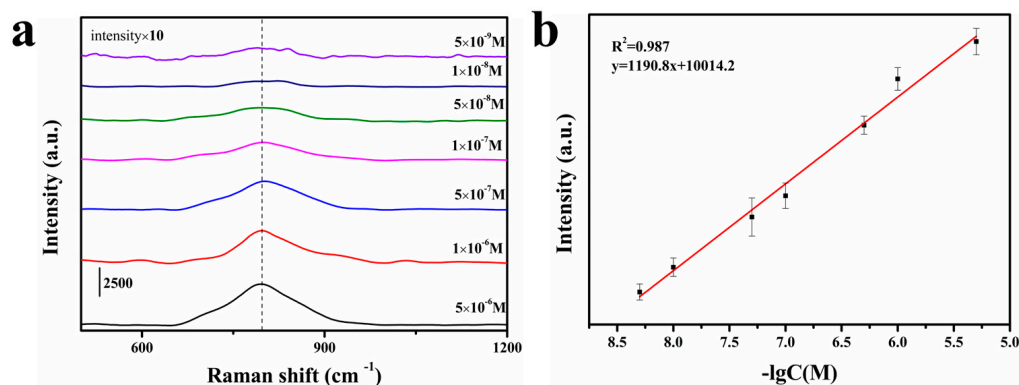


Figure 7. (a) SERS spectra of different concentrations of Cr(VI) in aqueous solution on the UIO-66/Ag/TiO₂. (b) Plot of SERS intensity at 798 cm⁻¹ versus logarithmic Cr(VI) concentration.

To evaluate the stability of the proposed substrate, we continuously monitored the SERS signals of Cr(VI) obtained on UIO-66/Ag/TiO₂ for 6 weeks to verify its practical application. The material was stored at room temperature. The variation of the characteristic peak intensity of Cr(VI) at 798 cm⁻¹ (5×10^{-7} M) over 6 weeks is shown in Figure 8. The SERS signal intensity hardly changed in 4 weeks. However, the average SERS intensity of the characteristic peaks decreased by 40.5% after 6 weeks of storage. These data fully demonstrate that UIO-66/Ag/TiO₂ as a SERS substrate has the dual advantages of high activity and good stability due to the synergistic effect of the components. Therefore, the substrate has great potential for the sensitive detection of Cr(VI) ions in environmental samples.

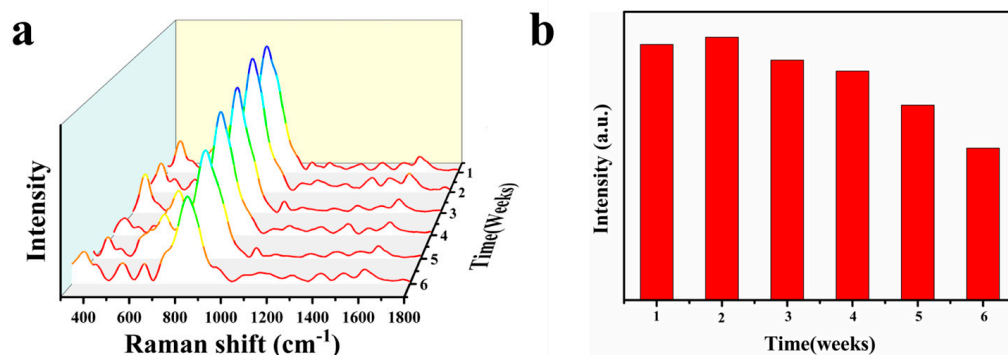


Figure 8. (a) Average intensities of Cr(VI) aqueous solution (5×10^{-7} M) peaks at 798 cm⁻¹ in 6 weeks. (b) Bar chart of peaks at 798 cm⁻¹.

Common anions, such as CO₃²⁻, SO₄²⁻, Cl⁻ and NO₃⁻, always coexist in real water. Thus, we performed SERS detection of Cr(VI) in the presence of CO₃²⁻, SO₄²⁻, Cl⁻ and NO₃⁻. Compared with the SERS spectra of standard Cr(VI) solution, Figure 9 shows that SERS intensity of Cr(VI) was slightly reduced in the presence of other anions due to the competitive adsorption of coexisting ions on the active site of the UIO-66/Ag/TiO₂ surface. However, the peak position of Cr(VI) only shows little shifts, indicating that the presence of other anions did not interfere with the identification of Cr(VI) significantly. Therefore, UIO-66/Ag/TiO₂ can effectively sense Cr(VI) in complex water systems. Taken

together, these experimental results indicate that UIO-66/Ag/TiO₂ is well suited for the quantitative detection of Cr(VI) in aqueous solutions.

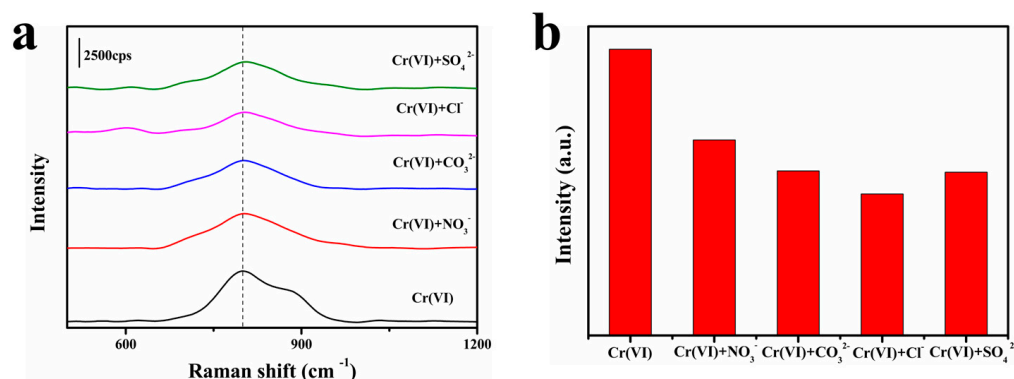


Figure 9. (a) SERS intensities at 798 cm⁻¹ of 5 × 10⁻⁶ M Cr(VI) aqueous solution in the presence of CO₃²⁻, SO₄²⁻, Cl⁻ and NO₃⁻ at 5 × 10⁻⁶ M; (b) bar chart of peaks at 798 cm⁻¹.

In order to verify the feasibility of the substrate for detecting the ion in real samples, a known concentration of Cr(VI) (5 × 10⁻⁶–10⁻⁷ M) was added to the samples using local lake water as the actual sample for detection. As shown in Figure 10, the substrate maintained a good linear relationship with the Cr(VI) ion concentration (R² = 0.912), but the lowest detection concentration of Cr(VI) in the actual sample was significantly higher than that in the standard solution. This result can be attributed to the competitive adsorption of Cr(VI) with other coexisting components in the lake water, blocking some hot spots that enhance the signal of Cr(VI) ions. The comparison of different nanomaterials for Cr(VI) and SERS activity is given in Table 1. The SERS activity of the prepared UIO-66/Ag/TiO₂ nanocomposites was slightly higher than that of the other reported substrates. It is worth mentioning that the three magnetic SERS substrates in studies 40, 32 and 20 show excellent SERS sensitivity, but the substrates need to be assembled by magnetic fields for SERS analysis and are solid-phase, which may lead to poor reproducibility of the SERS signal. In study 9, the LSPR effect of the two-layer AgNPs and the specific adsorption ability of ZrO₂ on Cr(VI) made the material robust for detection, but the unstable AgNPs exposed to the outer layer could not cope with the various factors in the actual sample. In study 40, the corresponding Cr(VI) concentration was obtained by impeding the binding of TiO₂-ARS (Alizarin Red S) by Cr(VI) ions, which reduced the intrinsic signal of ARS. Such a detection method not only has poor detection limits but also has poor ion interference. The above results suggest that UIO-66/Ag/TiO₂ nanocomposites have great potential for the practical monitoring of environmental contaminants.

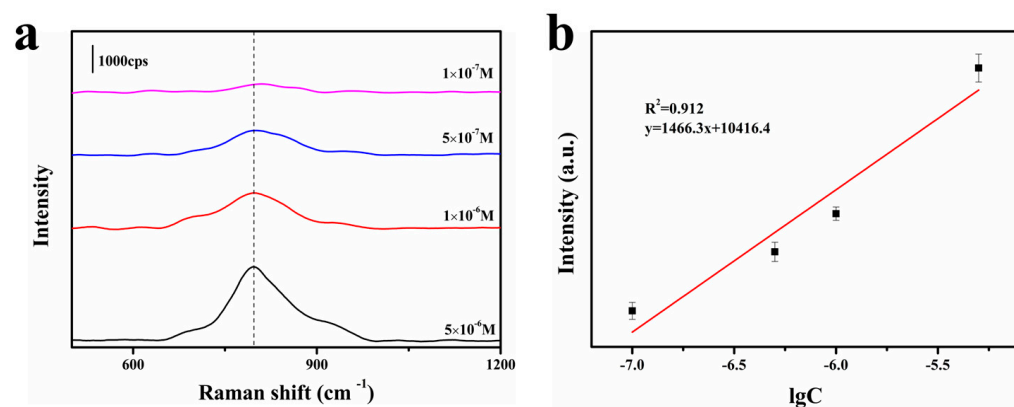


Figure 10. (a) SERS spectrum of lake water after mixing with UIO-66/Ag/TiO₂. (b) Plot of logarithmic SERS intensity at 798 cm⁻¹ versus logarithmic Cr(VI) concentration.

Table 1. Comparison of previously reported SERS substrates for Cr(VI) detection.

| Substrate | Detection Limit (μM) | Reference |
|--------------------------------------------------|-----------------------------------|-----------|
| $\text{Fe}_3\text{O}_4@\text{Ag}$ | 0.1 | [39] |
| $\text{Ag}@\text{ZrO}_2@\text{Ag}$ | 0.5 | [9] |
| $\text{Fe}_3\text{O}_4\text{-Au}@\text{TiO}_2$ | 0.05 | [29] |
| ARS- TiO_2 | 0.6 | [28] |
| $\text{Fe}_3\text{O}_4@m\text{-ZrO}_2@\text{Ag}$ | 0.05 | [22] |
| UIO-66/Ag/ TiO_2 | 0.005 | This work |

4. Conclusions

In this work, a new ternary composite UIO-66/Ag/ TiO_2 was proposed for the sensitive SERS detection of Cr(VI) in water samples. The composite combines the merits of the three components: UIO-66 can enhance the adsorption to Cr and provide a large area for AgNP loading, AgNPs produce a great electromagnetic enhancement effect amplifying the SERS signal, and TiO_2 can further significantly enhance the adsorption to Cr(VI). By adjusting the volume of the TiO_2 colloid, an optimized UIO-66/Ag/ TiO_2 with excellent SERS sensitivity was prepared for the sensitive SERS detection of Cr(VI) in water samples. The lowest detection concentration for Cr(VI) was 5 nM in a standard solution and 0.5 μM in a real lake water sample, both of which are lower than the allowable limit of Cr(VI) in drinking water (1 μM) set by the U.S. EPA. In addition, the UIO-66/Ag/ TiO_2 nanomaterials exhibited excellent storage stability. Therefore, the prepared UIO-66/Ag/ TiO_2 nanomaterials have important potential applications for the effective detection of environmental contaminants.

Author Contributions: Z.B.: conceptualization, investigation, writing—original draft preparation; G.M.: formal analysis, writing—review and editing; F.X.: supervision, writing—review and editing. All authors have read and agreed to the published version of the manuscript.

Funding: This research was funded by the National Natural Science Foundation of China, grant numbers 22264017 and 21705063.

Institutional Review Board Statement: Not applicable.

Informed Consent Statement: Not applicable.

Data Availability Statement: Data supporting reported results can be found from the authors.

Conflicts of Interest: The authors declare no conflict of interest.

References

- Murali, A.; Sarswat, P.K.; Free, M.L. Adsorption-coupled reduction mechanism in ZnO-Functionalized MWCNTs nanocomposite for Cr(VI) removal and improved anti-photocorrosion for photocatalytic reduction. *J. Alloys Compd.* **2020**, *843*, 155835. [CrossRef]
- Maitlo, H.A.; Kim, K.-H.; Kumar, V.; Kim, S.; Park, J.-W. Nanomaterials-based treatment options for chromium in aqueous environments. *Environ. Int.* **2019**, *130*, 104748. [CrossRef] [PubMed]
- Dawodu, F.A.; Akpan, B.M.; Akpomie, K.G. Sequestered capture and desorption of hexavalent chromium from solution and textile wastewater onto low cost *Heinsia crinita* seed coat biomass. *Appl. Water Sci.* **2020**, *10*, 32. [CrossRef]
- Arellano-Sánchez, M.G.; Devouge-Boyer, C.; Hubert-Roux, M.; Afonso, C.; Mignot, M. Quantitative extraction of chromium VI and III from tanned leather: A comparative study of pretreatment methods. *J. Leather Sci. Eng.* **2021**, *3*, 30. [CrossRef]
- Kazi, F.K.M.; Cooper, P.A. Method to recover and reuse chromated copper arsenate wood preservative from spent treated wood. *Waste Manag.* **2006**, *26*, 182–188. [CrossRef]
- Lee, C.-G.; Lee, S.; Park, J.-A.; Park, C.; Lee, S.J.; Kim, S.-B.; An, B.; Yun, S.-T.; Lee, S.-H.; Choi, J.-W. Removal of copper, nickel and chromium mixtures from metal plating wastewater by adsorption with modified carbon foam. *Chemosphere* **2017**, *166*, 203–211. [CrossRef]
- Motora, K.G.; Wu, C.-M. Magnetically separable highly efficient full-spectrum light-driven $\text{WO}_2.72/\text{Fe}_3\text{O}_4$ nanocomposites for photocatalytic reduction of carcinogenic chromium (VI) and organic dye degradation. *J. Taiwan Inst. Chem. Eng.* **2020**, *117*, 123–132. [CrossRef]
- Shakya, A.; Agarwal, T. Removal of Cr(VI) from water using pineapple peel derived biochars: Adsorption potential and re-usability assessment. *J. Mol. Liq.* **2019**, *293*, 111497. [CrossRef]
- Zhou, L.; Yang, J.; Wang, X.; Song, G.; Lu, F.; You, L.; Li, J. Ag nanoparticles decorated $\text{Ag}@\text{ZrO}_2$ composite nanospheres as highly active SERS substrates for quantitative detection of hexavalent chromium in waste water. *J. Mol. Liq.* **2020**, *319*, 114158. [CrossRef]

10. Fan, W.; Qiao, J.; Guan, X. Multi-wavelength spectrophotometric determination of Cr(VI) in water with ABTS. *Chemosphere* **2017**, *171*, 460–467. [[CrossRef](#)] [[PubMed](#)]
11. Ohira, S.-I.; Nakamura, K.; Chiba, M.; Dasgupta, P.K.; Toda, K. Matrix isolation with an ion transfer device for interference-free simultaneous spectrophotometric determinations of hexavalent and trivalent chromium in a flow-based system. *Talanta* **2017**, *164*, 445–450. [[CrossRef](#)]
12. Liu, X.; Li, T.; Wu, Q.; Yan, X.; Wu, C.; Chen, X.; Zhang, G. Carbon nanodots as a fluorescence sensor for rapid and sensitive detection of Cr(VI) and their multifunctional applications. *Talanta* **2017**, *165*, 216–222. [[CrossRef](#)] [[PubMed](#)]
13. Spanu, D.; Monticelli, D.; Binda, G.; Dossi, C.; Rampazzi, L.; Recchia, S. One-minute highly selective Cr(VI) determination at ultra-trace levels: An ICP-MS method based on the on-line trapping of Cr(III). *J. Hazard. Mater.* **2021**, *412*, 125280. [[CrossRef](#)] [[PubMed](#)]
14. Fakhriyan, G.; Mousavi, H.Z.; Sajjadi, S.M. Speciation and determination of Cr(III) and Cr(VI) by directly suspended droplet microextraction coupled with flame atomic absorption spectrometry: An application of central composite design strategy as an experimental design tool. *Anal. Methods* **2016**, *8*, 5070–5078. [[CrossRef](#)]
15. Wang, Y.; Ma, Y.; Zhao, Q.; Hou, L.; Han, Z. Polyoxometalate-based crystalline catalytic materials for efficient electrochemical detection of Cr(VI). *Sens. Actuators B Chem.* **2020**, *305*, 127469. [[CrossRef](#)]
16. Guo, L.; Tang, H.; Wang, X.; Yuan, Y.; Zhu, C. Nanoporous Ag-Decorated Ag₇O₈NO₃ Micro-Pyramids for Sensitive Surface-Enhanced Raman Scattering Detection. *Chemosensors* **2022**, *10*, 539. [[CrossRef](#)]
17. Song, Y.; Xiao, K.; Chen, Q.; Zhang, X.; Yu, Z.; Chen, W.; Zhang, X.; Zhang, D.; Ni, D.; Liang, P. Fabrication of GO/Fe₃O₄@Au MNPs for Magnetically Enriched and Adsorptive SERS Detection of Bifenthrin. *Chemosensors* **2023**, *11*, 73. [[CrossRef](#)]
18. Wang, D.; Hui, B.; Zhang, X.; Zhu, J.; Gong, Z.; Fan, M. Facile Preparation of Ag-NP-Deposited HRGB-SERS Substrate for Detection of Polycyclic Aromatic Hydrocarbons in Water. *Chemosensors* **2022**, *10*, 406. [[CrossRef](#)]
19. Zhu, J.; Wang, B.; Yang, P.; Li, J.; Xiao, G.; Yao, J.; Gong, X.; Yan, J.; Zhang, H. The Functional Fe₃O₄@SiO₂@AuNPs SERS Nanomaterials for Rapid Enrichment and Detection of Mercury Ions in Licorice. *Chemosensors* **2022**, *10*, 403. [[CrossRef](#)]
20. Long, Y.; Li, H.; Wang, W.; Yang, X.; Liu, Z. Ultrasensitive detection of Cr(VI) using a novel SERS optical fiber probe modified by dual-functional methimazole. *J. Alloys Compd.* **2022**, *910*, 164916. [[CrossRef](#)]
21. Xu, G.; Guo, N.; Zhang, Q.; Wang, T.; Song, P.; Xia, L. A sensitive surface-enhanced resonance Raman scattering sensor with bifunctional negatively charged gold nanoparticles for the determination of Cr(VI). *Sci. Total Environ.* **2022**, *830*, 154598. [[CrossRef](#)]
22. Wang, X.; Cheng, H.; Min, Y.; Li, X.; You, L.; Li, J. Fe₃O₄@m-ZrO₂@Ag ternary magnetic nanocomposites for sensitive SERS sensing and photocatalytic removal of Cr(VI) and organic dyes. *Compos. Part B Eng.* **2022**, *239*, 109959. [[CrossRef](#)]
23. Wang, C.; Shang, M.; Wei, H.; Zhang, M.; Zou, W.; Meng, X.; Chen, W.; Shao, H.; Lai, Y. Specific and sensitive on-site detection of Cr(VI) by surface-enhanced Raman spectroscopy. *Sens. Actuators B Chem.* **2021**, *346*, 130594. [[CrossRef](#)]
24. Wang, Q.; Zhao, Y.; Bu, T.; Wang, X.; Xu, Z.; Zhangsun, H.; Wang, L. Semi-sacrificial template growth-assisted self-supporting MOF chip: A versatile and high-performance SERS sensor for food contaminants monitoring. *Sens. Actuators B Chem.* **2021**, *352*, 131025. [[CrossRef](#)]
25. Sun, Y.; Yu, X.; Hu, J.; Zhuang, X.; Wang, J.; Qiu, H.; Ren, H.; Zhang, S.; Zhang, Y.; Hu, Y. Constructing a Highly Sensitivity SERS Sensor Based on a Magnetic Metal–Organic Framework (MOF) to Detect the Trace of Thiabendazole in Fruit Juice. *ACS Sustain. Chem. Eng.* **2022**, *10*, 8400–8410. [[CrossRef](#)]
26. Luo, M.; Xiong, Y.; Wu, H.; Feng, X.; Li, J.; Feng Luo, F. MOF + Technique Showing Significant Synergic Effect and thus Enabling Super-Performance in the Chromate Removal. *Angew. Chem. Int. Ed.* **2017**, *51*, 16376–16379. [[CrossRef](#)]
27. Liu, J.; Ye, Y.; Sun, X.; Liu, B.; Li, G.; Liang, Z.; Liu, Y. A multifunctional Zr(IV)-based metal–organic framework for highly efficient elimination of Cr(VI) from the aqueous phase. *J. Mater. Chem. A* **2019**, *7*, 16833–16841. [[CrossRef](#)]
28. Ji, W.; Wang, Y.; Tanabe, I.; Han, X.; Zhao, B.; Ozaki, Y. Semiconductor-driven “turn-off” surface-enhanced Raman scattering spectroscopy: Application in selective determination of chromium(VI) in water. *Chem. Sci.* **2015**, *6*, 342–348. [[CrossRef](#)]
29. Lv, B.; Sun, Z.; Zhang, J.; Jing, C. Multifunctional satellite Fe₃O₄-Au@TiO₂ nano-structure for SERS detection and photo-reduction of Cr(VI). *Colloids Surf. Physicochem. Eng. Asp.* **2017**, *513*, 234–240. [[CrossRef](#)]
30. Xu, H.; Zhu, J.; Cheng, Y.; Cai, D. Functionalized UiO-66@Ag nanoparticles substrate for rapid and ultrasensitive SERS detection of di-(2-ethylhexyl) phthalate in plastics. *Sens. Actuators B Chem.* **2021**, *349*, 130793. [[CrossRef](#)]
31. Wang, X.; Chen, W.; Zhang, L.; Yao, T.; Liu, W.; Lin, Y.; Ju, H.; Dong, J.; Zheng, L.; Yan, W.; et al. Uncoordinated Amine Groups of Metal–Organic Frameworks to Anchor Single Ru Sites as Chemoselective Catalysts toward the Hydrogenation of Quinoline. *J. Am. Chem. Soc.* **2017**, *139*, 9419–9422. [[CrossRef](#)] [[PubMed](#)]
32. Prathapani, S.; More, V.; Bohm, S.; Bhargava, P.; Yella, A.; Mallick, S. TiO₂ colloid-based compact layers for hybrid lead halide perovskite solar cells. *Appl. Mater. Today* **2017**, *7*, 112–119. [[CrossRef](#)]
33. Cao, J.; Yang, Z.; Xiong, W.; Zhou, Y.; Peng, Y.; Li, X.; Zhou, C.; Xu, R.; Zhang, Y. One-step synthesis of Co-doped UiO-66 nanoparticle with enhanced removal efficiency of tetracycline: Simultaneous adsorption and photocatalysis. *Chem. Eng. J.* **2018**, *353*, 126–137. [[CrossRef](#)]
34. Wang, Y.; Liu, H.; Zhang, M.; Duan, W.; Liu, B. A dual-functional UiO-66/TiO₂ composite for water treatment and CO₂ capture. *RSC Adv.* **2017**, *7*, 16232–16237. [[CrossRef](#)]
35. Zhang, R.; Du, B.; Li, Q.; Cao, Z.; Feng, G.; Wang, X. α-Fe₂O₃ nanoclusters confined into UiO-66 for efficient visible-light photodegradation performance. *Appl. Surf. Sci.* **2019**, *466*, 956–963. [[CrossRef](#)]

36. Xu, H.; Shi, X.; Ma, H.; Lv, Y.; Zhang, L.; Mao, Z. The preparation and antibacterial effects of dopa-cotton/AgNPs. *Appl. Surf. Sci.* **2011**, *257*, 6799–6803. [[CrossRef](#)]
37. Ma, Y.; Tang, Q.; Sun, W.-Y.; Yao, Z.-Y.; Zhu, W.; Li, T.; Wang, J. Assembling ultrafine TiO₂ nanoparticles on UiO-66 octahedrons to promote selective photocatalytic conversion of CO₂ to CH₄ at a low concentration. *Appl. Catal. B Environ.* **2020**, *270*, 118856. [[CrossRef](#)]
38. Athira, T.; Roshith, M.; Babu, T.S.; Kumar, D.V.R. Fibrous red phosphorus as a non-metallic photocatalyst for the effective reduction of Cr(VI) under direct sunlight. *Mater. Lett.* **2020**, *283*, 128750. [[CrossRef](#)]
39. Du, J.; Jing, C. Preparation of Fe₃O₄@Ag SERS substrate and its application in environmental Cr(VI) analysis. *J. Colloid Interface Sci.* **2011**, *358*, 54–61. [[CrossRef](#)]

Disclaimer/Publisher's Note: The statements, opinions and data contained in all publications are solely those of the individual author(s) and contributor(s) and not of MDPI and/or the editor(s). MDPI and/or the editor(s) disclaim responsibility for any injury to people or property resulting from any ideas, methods, instructions or products referred to in the content.